(Received 11 February 2025, Accepted 23 May 2025, Scheduled 22 July 2025)

The Electromagnetic Distribution and Intelligent Signal Extraction of ELF-EM in Hole-Ground Communication

Fukai Li[1,2,*], Yue Zhao[1,2], Wei Guo[2], Jian Wu[1,2], Zan Yin[2], Huaiyun Peng[1,2], and Kai Liu[1,2]

[1] *National Key Laboratory of Electromagnetic Environment, Research Institute of Radiowave Propagation, Qingdao 266109, China*
[2] *China Research Institute of Radiowave Propagation, Qingdao 266109, China*

ABSTRACT: In the field of drilling engineering, innovations in drilling communication (also known as hole-ground communication while drilling) technology are crucial for enhancing exploration efficiency, ensuring operational safety, and optimizing data collection. Extremely Low Frequency electromagnetic (ELF-EM) wave communication transmission technology, with its exceptional penetration capability in formations and low attenuation characteristics, is emerging as a key technology in drilling communications. However, this technology faces challenges such as complex transmission model calculations and difficulty in extracting weak signals from the ground, which hinder its further development. Addressing issues like the inability of conventional models to accurately describe nonuniform media, low frequencies, and near-field open-space conditions in ELF-EM transmission under drilling conditions, as well as numerical dispersion, this paper innovatively conducts a comprehensive and systematic analysis of electromagnetic distribution in extended-reach horizontal wells using the finite element modeling and analysis method. Through software simulations and field tests, the following conclusions are drawn: The induced current on the drill pipe plays a major role in the ground field distribution and the signal received by the system terminal; the horizontal drill pipe in a horizontal well has a certain impact on the ground-received signal, mainly manifesting in that the orientation of the ground-receiving electrode should align with the direction of the horizontal well, and the larger the azimuth difference is from the drilling direction, the smaller the signal reception is; at the surface of the drilling platform, not only can multiple electrodes be used to receive signals, but magnetic sensors can also be employed to receive magnetic component signals. Addressing the issue of extracting communication signals in complex electromagnetic environments during electromagnetic measurement-while-drilling (EM-MWD) operations, a multi-channel intelligent signal extraction method has been designed. This method can improve the in-band signal-to-noise ratio (SNR) by more than 3 to 5 dB and further extend the communication transmission distance compared to single-channel models.

1. INTRODUCTION

In the field of drilling engineering, innovations in communication while drilling (CWD) technology are crucial for enhancing exploration efficiency, ensuring operational safety, and optimizing data collection. ELF-EM wave, with its exceptional penetration capabilities and low attenuation characteristics in formations, is gradually becoming a key technology in drilling communication [1, 2]. This paper aims to delve into the electromagnetic distribution patterns of ELF-EM wave during drilling communication processes and explore how advanced signal processing techniques can be used for intelligent signal extraction, thereby providing stable and reliable communication support for drilling operations. ELF-EM wave primarily transmits through the channel composed of drill pipes, casings, drilling media, and formations during the drilling process [3]. Signal transmission is influenced by various factors such as formation structure, drilling media conductivity, electromagnetic wave frequency, resulting in complex and variable electromagnetic distribution characteristics (Figure 1). Traditional methods mainly include transmission line method [4], numerical methods [5], and equivalent circuit method [6, 7]. Drilling electromagnetic wave transmission belongs to the open-field problem of nonuniform media and ELF near fields. The distribution of the electromagnetic field in the near-field region is closely related to the current distribution on the antenna. Therefore, the accuracy of field calculations is constrained by the precision of solving the current distribution on the antenna [8]. Current theoretical research primarily relies on theoretical models established based on the equivalent transmission line

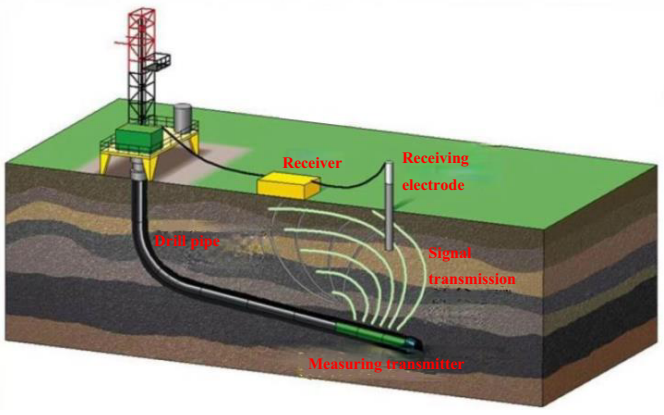

FIGURE 1. ELF electromagnetic wave wireless communication scenario in drilling.

* Corresponding author: Fukai Li (lfkai@foxmail.com).

method. Although this method can consider both radial and longitudinal stratification of surrounding media when solving for the current distribution on the antenna, it adopts calculations for vertical electric dipoles in longitudinally stratified media when solving for ground field strength, implicitly treating the antenna as a thin wire and neglecting its radial dimensions. Additionally, this method does not account for the influence of boreholes and mud when solving for ground fields, thus failing to describe some detailed issues [9], such as the analysis of how the length of the insulated portion of asymmetric dipole antennas affects signal magnitude. When numerical methods are used to solve cross-medium boundary value problems, differential equation method is commonly employed, but it suffers from numerical dispersion issues. When electric field integral equations are used for ELF calculations, due to decoupling effects between electric and magnetic fields, low-frequency collapse can easily occur during numerical calculations [10]. Furthermore, current theoretical research mostly focuses on vertically oriented boreholes in axially symmetric media, with no in-depth studies on inclined and horizontal boreholes, particularly the impact of horizontal boreholes on the distribution of ground fields. To address the challenges of precisely describing the nonuniform media, low-frequency, near-field open-field model of drilling electromagnetic wave transmission and numerical dispersion, this paper conducts a systematic comprehensive analysis of extended-reach horizontal wells from the perspective of the finite element modeling and analysis method, deriving favorable ground signal reception methods under different conditions. The finite element modeling and analysis method for drilling electromagnetic waves establishes numerical models incorporating parameters such as formation conductivity, resistivity, and media characteristics, and divides the solution region into a grid, dividing the continuous formation into several small units. Partial differential equations or integral equations for electromagnetic waves are established on each unit, and these equations are solved using the finite element method to obtain approximate solutions for field variables (such as electric field intensity and magnetic field intensity) on each unit. These approximate solutions are then connected in a certain way between units to form the distribution of field variables across the entire solution domain. Through finite element analysis of drilling electromagnetic waves, the propagation process of electromagnetic waves in formations can be simulated, including various aspects such as electromagnetic wave emission, transmission, attenuation, and reception. In addition, due to factors such as field operations and formation conductivity in drilling engineering that cause attenuation and interference to electromagnetic wave signals, the received ELF signals often contain a large amount of noise and interference components. When ELF wireless communication signals are transmitted from within the borehole through the formation to the ground, the terminal reception signals inevitably pick up various types of noise, most of which are colored low-frequency noise such as electromechanical power frequencies, electromagnetic effects produced by mechanical vibrations, or other external interference. As the drilling electromagnetic wave wireless communication distance increases, signals become weaker, and the SNR deteriorates. The inclusion of many non-stationary signals and nonlinear noise signals, such as abrupt terms, ultimately makes detection and decoding difficult. One of the key technologies to improve communication capabilities is how to better recover the original signal from the "noisy" signal. To address the challenge of enhancing the SNR at the EM reception terminal while drilling, relevant research institutions and universities have conducted extensive research. For example, Long et al. proposed a harmonic interference elimination algorithm based on sine wave parameter estimation [11]. This algorithm is primarily targeted at power frequency harmonic interference and requires harmonic signal reconstruction, leading to poor real-time performance and inability to meet the requirements of extracting electromagnetic wave signals in complex noise environments on site. Wang et al. proposed an EM-MWD signal detection algorithm based on a correlation adapter [12]. This algorithm detects the similarity between signals and noise based on their statistical properties. Correlation detection techniques are typically used to extract signals. However, this algorithm does not provide a good explanation for how to collect noise sources for adaptive correlation filtering. Usually, noise and signals are within the same transmission channel, making it impossible to separately collect and analyze them, thus failing to meet the prerequisites for this algorithm. Fayemi et al. proposed the design of an EM-MWD receiver based on a neural network algorithm [13]. Neural network receivers have adaptive learning capabilities and outperform correlation receivers under various noise conditions, especially in the presence of non-white noise and real-world noise obtained from actual drilling sites. However, ELF-EM signals have high engineering real-time requirements, and field noise exhibits non-stationary characteristics (requiring continuous training based on noise characteristics). Therefore, adopting neural network algorithms cannot meet the requirements of engineering sites. Lu et al. utilized adjacent well data for signal extraction [14]. This method has certain limitations and does not fully consider the electromagnetic wave distribution in horizontal well conditions, as well as interference from the surrounding complex electromagnetic environment. In summary, the above methods have certain limitations or inadequate in-band denoising effects, making it difficult to meet the requirements for the transmission depth of drilling electromagnetic waves. Therefore, research on improving the SNR of ELF signals received at the terminal, especially the SNR of in-band noise, has become one of the key issues for breaking through the transmission distance limit of drilling electromagnetic waves.

2. ELF CHANNEL CHARACTERISTICS AND AMBIENT NOISE UNDER DRILLING CONDITIONS

2.1. Analysis of Factors Influencing ELF Subsurface Transmission

The primary factors influencing ELF reception at the ground surface are electrical conductivity σ, magnetic permeability μ, and permittivity ε. For most media (excluding ferromagnetic media), the magnetic permeability μ is similar to that in a vacuum (approximately $4\pi \times 10^{-7}$ H/m). ε and σ can be repre-

sented using complex permittivity or complex conductivity, respectively.

$$\varepsilon^* = \varepsilon + j\frac{\sigma}{\omega} \quad \sigma^* = \sigma - j\omega\varepsilon \tag{1}$$

The carrier frequencies for ELF communication in drilling operations typically range from a few Hz to a dozen Hz. At these frequencies, $\sigma \gg \omega\varepsilon$, making electrical conductivity (or resistivity) the primary factor influencing the communication performance of electromagnetic wave transmission systems in drilling [15].

The transmission of ELF-EM wave in formations during drilling can be affected by various factors, which may lead to attenuation or changes in the electromagnetic waves, thereby influencing the quality and stability of the signals. The main influencing factors are as follows:

Formation conductivity: The conductivity of formations has a significant impact on the propagation of electromagnetic waves. Conductivity is closely related to factors such as mineral composition, water content, porosity, temperature, pressure, frequency, and polarization intensity of the formations. For example, formations with high water content and porosity tend to have higher conductivity, which may lead to increased energy loss during the propagation of electromagnetic waves. Therefore, the distribution and variation of formation conductivity directly affect the propagation characteristics of electromagnetic waves.

Formation resistivity: Formation resistivity is a key factor influencing the signal transmission of EM-MWD systems. When the formation resistivity is very low (e.g., less than 1 unit), electromagnetic signals tend to attenuate easily and are difficult to transmit to the surface. Conversely, when the formation resistivity is very high (e.g., greater than 200 unit), electromagnetic signals may be blocked, preventing the completion of signal transmission. Therefore, when selecting electromagnetic wave excitation and transmission methods, the range of formation resistivity needs to be considered.

Formation medium characteristics: When electromagnetic waves propagate through formations, the medium characteristics of the formations, such as rock type, particle size, density, and distribution, all influence the propagation of electromagnetic waves. Different formation media exhibit different absorption, reflection, and refraction characteristics for electromagnetic waves, which may result in energy loss and waveform changes during the propagation process.

Frequency and wavelength: The frequency and wavelength of electromagnetic waves also play important roles during propagation. Different frequencies and wavelengths correspond to different penetration capabilities and transmission speeds. Lower-frequency electromagnetic waves may have better penetration capabilities but slower transmission speeds, whereas higher-frequency electromagnetic waves, although they are faster in transmission, may have poorer penetration capabilities. Therefore, when selecting electromagnetic wave frequency bands, it is necessary to comprehensively consider formation characteristics and operational requirements.

In summary, the transmission of drilling electromagnetic waves in formations is affected by multiple factors that intertwine and act together. To ensure stable and effective transmission of electromagnetic signals, it is necessary to conduct in-depth research on formation characteristics and select appropriate electromagnetic wave excitation and transmission methods. Additionally, technical means should be employed to enhance and correct signals to overcome the adverse effects during transmission through formations.

2.2. Computational Simulation

Finite element analysis for drilling electromagnetic waves is a method used to simulate and predict the propagation characteristics of drilling electromagnetic waves in formations. Finite element analysis is a numerical calculation method that discretizes the continuous solution domain into a finite set of elements, applying approximate mathematical expressions on each element to describe the variation of field variables.

In finite element analysis for drilling electromagnetic waves, the first step is to establish a numerical model of the formation, which considers parameters such as conductivity, resistivity, and medium properties of the formation. Subsequently, the solution area is meshed, dividing the continuous formation into several small elements. On each element, based on electromagnetic field theory, partial differential equations or integral equations for electromagnetic waves are established. Next, these equations are solved using the Finite Element Method to obtain approximate solutions for field variables (such as electric field intensity and magnetic field intensity) on each element. These approximate solutions are connected in a certain way between elements to form the field variable distribution across the entire solution domain. Through finite element analysis for drilling electromagnetic waves, the propagation process of electromagnetic waves in formations can be simulated, including the emission, propagation, attenuation, and reception of electromagnetic waves, which aids in predicting the propagation characteristics of electromagnetic wave signals under different formation conditions, such as signal strength, phase, and propagation speed. Additionally, finite element analysis can be used to study the impact of formation parameters on electromagnetic wave propagation. By adjusting the parameters of the formation model, the propagation of electromagnetic waves under different formation conditions can be simulated, further analyzing the influence patterns of factors such as formation conductivity and resistivity on electromagnetic wave propagation [16]. Finite element analysis for drilling electromagnetic waves is an effective numerical calculation method for simulating and predicting the propagation characteristics of drilling electromagnetic waves in formations, providing theoretical support and guidance for actual drilling operations.

2.2.1. Finite Element Analysis Modeling and Computation

In practical drilling engineering, the ELF transmission medium is constantly changing, and variables such as electric field intensity and magnetic field intensity may be discontinuous, whereas classical electromagnetic field theory requires these variables to be continuously distributed. To address this issue, the introduction of curl variables is necessary [17]. The trans-

mission of drilling ELF signals in various formations should all satisfy Maxwell's equations, and the formula involving the curl in Maxwell's equations is:

$$\oint_l Hdl = \int_S JdS + \int_S \frac{\partial D}{\partial t} dS \tag{2}$$

$$\oint_l Edl = -\int_S \frac{\partial B}{\partial t} dS \tag{3}$$

where H (A/m) is the magnetic field intensity; l (m) is the length of the conductor loop; J (A/m^2) is the current density; S (m^2) is the area of the surface bounding the loop; t is the time; D (C/m^2) is the electric flux density; E (V/m) is the electric field intensity; B (Wb/m) is the magnetic flux density.

Based on the equivalent transmission line theory, both the upper and lower drill strings, serving as "transmission lines," are charged conductors that simultaneously radiate energy into the formation. It is necessary to calculate the potential changes in the drill strings and the formation separately, and then integrate the results to obtain the total potential change. On the other hand, the finite element analysis method essentially transforms the boundary value problem of solving differential equations into an equivalent variational problem of finding the extreme value of a functional. The field is then divided into a number of small elements, and the approximate solution to the original differential equation is obtained by solving for the extreme value in each small element [18]. The mathematical formula for this is:

$$b_k(\eta) = \sum_{i=1}^{n} b_i h(x) \quad (i = 1, 2, 3, \ldots, n) \tag{4}$$

In the formula, b_k is the approximate solution to the equation obtained for the specified element in the finite element analysis; η is the coordinate axis; b_i is the compensation coefficient; $h(x)$ is the extreme value of the calculation parameter in the finite element model; n is the number of mesh elements divided.

From Equations (2) and (3), the potential difference formula for conduction current in a conductive object can be derived:

$$V(x) = \int_0^l Edl = \int_0^l \frac{\mathbf{J}}{\sigma} dl \tag{5}$$

In the formula, $V(x)$ denotes the potential difference, with units of V, and σ denotes the electrical conductivity, with units of S/m.

In the space of vorticity, the following relationship exists for vector functions:

$$\nabla \cdot G(\eta) = \frac{\partial G_2(\eta_2)}{\partial \eta_1} - \frac{\partial G_1(\eta_1)}{\partial \eta_2} \tag{6}$$

where ∇ represents the Hamiltonian operator; $G(\eta)$ represents the vector function at point η in the finite element solution; η_1 and η_2 represent the vector functions at any two points in the finite element coordinates. By performing integral transformations on Equations (4), (5), and (6), and applying the finite element model, the potential difference between the two points is obtained as follows:

$$V(x) = \sum_{i=1}^{n} b_i \int_0^l \frac{\mathbf{J}_i - \mathbf{J}_{i-1}}{\sigma_i} dl \tag{7}$$

$\mathbf{J}_i$ and $\mathbf{J}_{i-1}$ represent the current densities at finite element nodes i and $i-1$ respectively, with units of A/m; σ_i represents the electrical conductivity at finite element node i, with units of S/m.

Based on the above theoretical analysis, to calculate the potential difference between two points, it is only necessary to integrate and sum the potential differences at each point along the downhole current loop. Based on this, a finite element analysis model can be established to simulate and analyze the impact on ELF signal transmission within the drill string.

(1) Model Establishment

The schematic diagram of the finite element method modeling and calculation model profile is shown in Figure 2. In Figure 2, 1 and 2 represent metal casings with a diameter of 20 cm; 1 is the casing for the vertical well section, and 2 is the casing for the horizontal section. The build-up section between 1 and 2 is a quarter-circle arc with a radius of curvature of 36 m. 3 is a 1-meter-long insulating joint located 50 meters ahead of the end of the casing. Region 4 represents the formation, which is the calculation area with dimensions set to 3000 m in length, 2000 m in width, and 2000 m in depth. To simulate a calculation area with infinite length, width, and depth, region 5 is set as an infinite element domain with a thickness of 100 m.

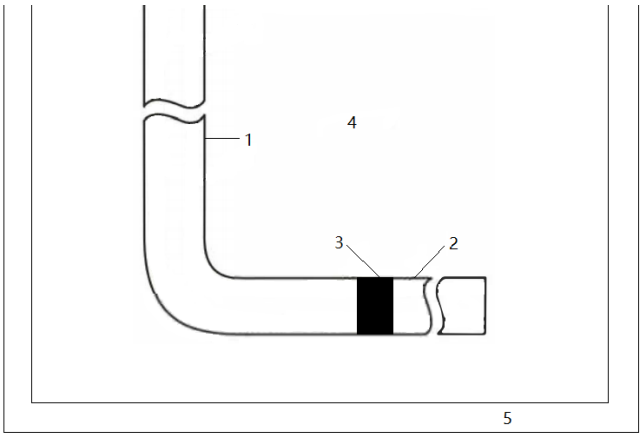

FIGURE 2. Schematic diagram of the model profile. 1 — vertical casing, 2 — horizontal casing, 3 — insulating joint, 4 — formation, 5 — infinite element domain.

The primary material of the casing in the model is steel, with a conductivity of 1.12×10^6 S/m. Under ideal conditions, the conductivity of the casing's insulating joint is set to 0 S/m. The model employs a homogeneous formation with a resistivity of $0.02\,\Omega \cdot$ m (note: resistivity is the reciprocal of conductivity, so 0.02 S/m should be converted to $\Omega \cdot$ m for consistency, but

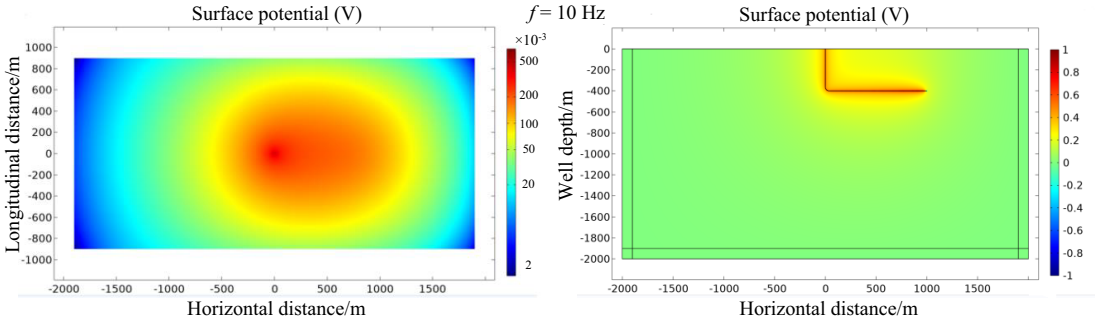

FIGURE 3. Scenario of a vertical hole with a depth of 400 meters and a horizontal hole extending 1000 meters.

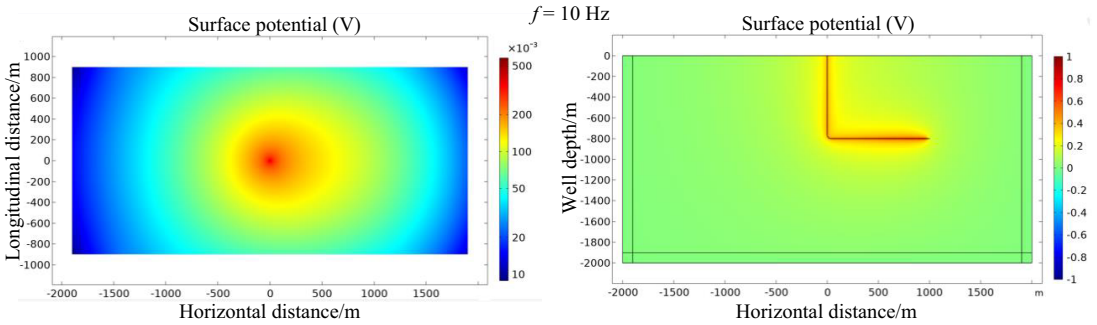

FIGURE 4. Scenario of a vertical hole with a depth of 800 meters and a horizontal hole extending 1000 meters.

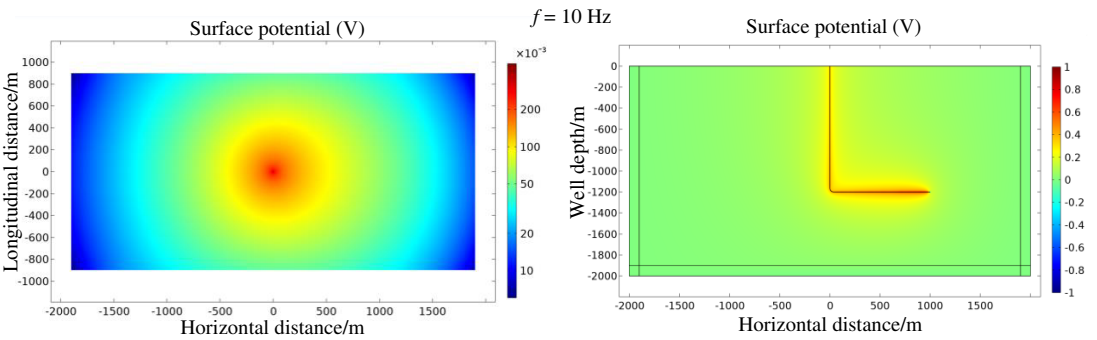

FIGURE 5. Scenario of a vertical hole with a depth of 1200 meters and a horizontal hole extending 1000 meters.

here it is kept as 0.02 S/m for simplicity in the context of this translation, understanding that it refers to the reciprocal value in practical terms). The model operates at a frequency of 10 Hz with a voltage excitation applied, specifically, $+1$ V and -1 V potentials are applied at both ends of the insulating joint, respectively.

The model employs tetrahedral mesh segmentation, addressing issues of poor mesh quality arising from the significant size difference between the formation model and the radial size of the casing by adjusting element growth rates and resolution in narrow areas. To enhance computational efficiency, the entire model, including the formation and casing, as depicted in the profile of Figure 2, is divided into two parts. The profile is set as an electrical symmetry plane, allowing for the calculation of only half of the region. This approach reduces the number of mesh elements by half, significantly decreasing the computational load and accelerating the calculation speed.

(2) Model Simulation and Calculation

This paper analyzes the construction environment of horizontal wells and calculates the distribution characteristics of the ground field. Based on the calculated electric and magnetic field distributions, the position of the receiving antenna is reasonably arranged to enhance the received signal strength. A BiGCStab iterative solver is employed to iteratively solve each mesh, with a set solution residual of 0.01. For the ELF transmission formation model during drilling, due to its large volume, adaptive meshing in Ansys is adopted in this paper. In this study, the AC/DC module in COMSOL software is used to simulate different combinations of straight and horizontal holes in horizontal drilling scenarios. The simulation and calculation results are shown in Figures 3–7.

(3) Experimental verification

In order to verify the correctness of theoretical model analysis, an experimental well data is selected to compare the measured value with the theoretical calculated value. Casing length of the experimental well is 274 m, casing size 320.4 mm, well

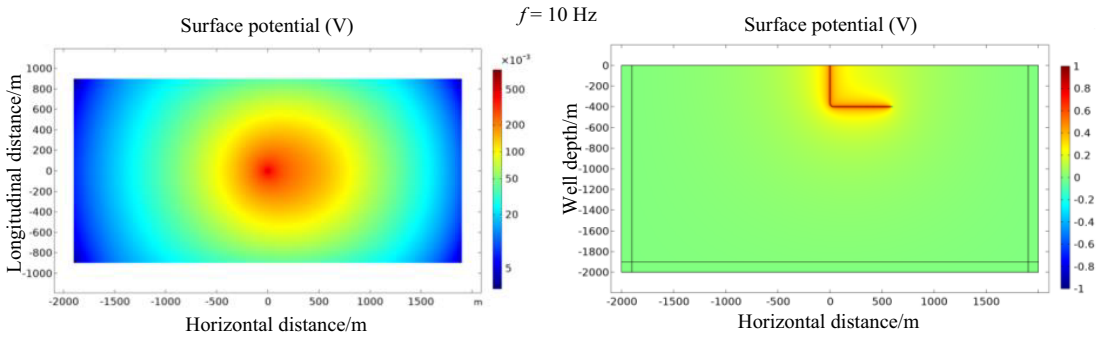

FIGURE 6. Scenario of a vertical hole with a depth of 400 meters and a horizontal hole extending 600 meters.

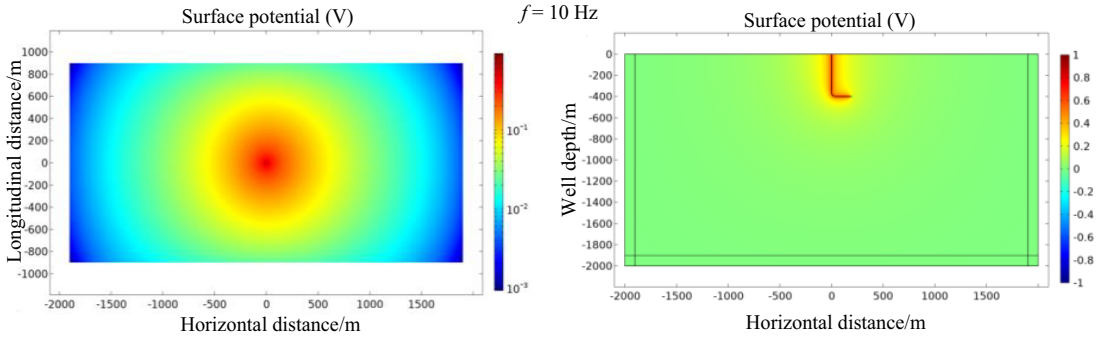

FIGURE 7. Scenario of a vertical hole with a depth of 400 meters and a horizontal hole extending 200 meters.

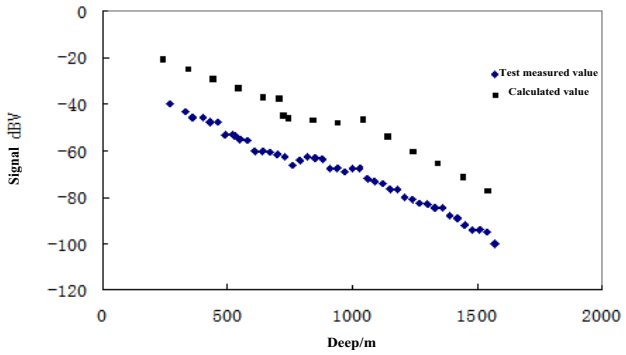

FIGURE 8. Comparison of calculated results and test results.

depth 3100 m, transmitting antenna 18 m, and ground receiving antenna 100 m. Take $0 \sim 1100$ m formation resistivity as $7\,\Omega \cdot$ m and 1100~2800 m formation resistivity as $2\,\Omega \cdot$ m. The excitation source power is 100 W, and the frequency is 10 Hz. See Figure 8 for the results of the concrete comparison. From the theoretical calculation and measured results, we can find that by comparing calculated value with measured value, the signal variation trend with depth has a good consistency, reflecting the actual formation of different resistivity stratifications, but the calculated value 20 dB is more than the measured value. This is because theoretical calculations take idealized models, while actual measurement will be influenced by contact resistance, approximate electrical resistivity and grounding resistance at the receiving end. This will inevitably result in the difference between theoretical calculation and measured value, but the theoretical model can basically reflect the real situation and provide the theoretical guidance for tool design.

2.2.2. The Influence of Receiver Electrode Orientation and Dipole Moment on the Terminal Received Signal

In vertical drilling, without the influence of horizontal sections, the ground-received signal increases with the increase of the dipole moment, but the rate of increase gradually diminishes until it stabilizes. With the advancement of drilling technology, extended-reach horizontal wells have become increasingly common in daily development. The ground-received signal is inevitably affected by the electrode orientation, dipole moment, and adjacent wells. A detailed analysis through simulations combined with experiments is shown below.

Assuming the wellhead location as the origin and the direction of the horizontal well at 0°, dipole moments with distances of 50 m, 100 m, 200 m, 400 m, 600 m, and 800 m are set in directions of 0°, −45°, −90°, −135°, and −180°, respectively, as illustrated in Figure 9 for reference.

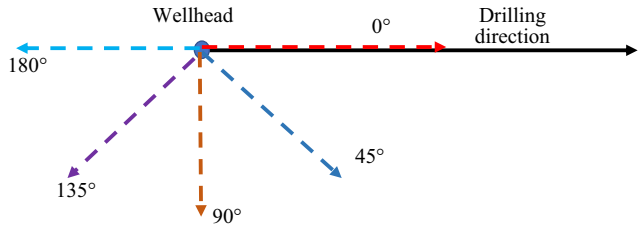

FIGURE 9. Schematic diagram of ground receiver electrode Orientation.

After finite element modeling and analysis, the following conclusions can be drawn: In the 3D model of horizontal wells, the surface-received electrode signals are symmetrically dis-

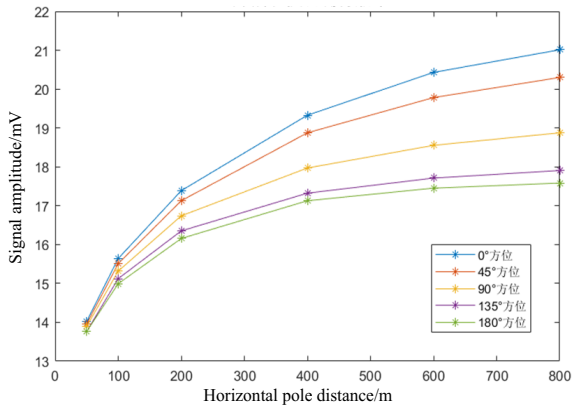

FIGURE 10. Electrode received signals for different azimuthal dipole moments.

tributed relative to the stratigraphic profile, and the signal field strength is maximized directly above the horizontal section in the same direction as the dipole moment. Figure 10 presents the theoretical simulation values for different orientations and dipole moment magnitudes. Here, the vertical well section is 1000 m long; the horizontal section is 1000 m long; and the conductivity is $1.12 * 10^6$ S/m. In ideal conditions, the conductivity of the casing insulating joint is set to 0 S/m. The model adopts a uniform stratum with a resistivity of 0.02 S/m. The model operates at a frequency of 10 Hz with a voltage excitation applied, specifically, and $+1$ V and -1 V potentials are applied at both ends of the insulating joint, respectively. From the results, the following conclusions can be drawn: (1) With the same dipole moment magnitude, the primary factor affecting signal magnitude is the dipole moment orientation. The larger the angular difference is from the horizontal section's orientation, the smaller the signal is, reaching a minimum at 180°, and the received signal magnitude is symmetrical about the horizontal section. (2) With the same orientation, the signal increases with the increase of the receiving dipole moment, but the rate of increase or slope gradually decreases until it plateaus. From an engineering perspective, when conditions permit, wiring for signal reception should be done as far as possible in the direction of the horizontal section.

The field test measurement signals are shown in Figure 11, with the red line representing the distal signal and the blue line representing the proximal signal. The distal point is located near the azimuthal direction, approximately 30 meters away from the wellhead, and the original signal has a peak-to-peak value of 0.020 V. The proximal point is in the vicinity of the instrument room, about 15 meters from the wellhead, with an original signal peak-to-peak value of 0.015 V. The comparison of signal amplitudes at the engineering site further verifies that the dipole azimuth and distance do have an impact on the received signals.

2.2.3. Impact of Adjacent Wells on Terminal Received Signals

To consider the impact of adjacent wells on received signals, let's assume that there is a completed adjacent well located in the direction of the horizontal section, as illustrated in Figure 12. Since the casing of the adjacent well is a good conductor, it inevitably has a certain impact on the distribution of the surface electromagnetic field. Below, we analyze the influence of the adjacent well on the surface EM field distribution through finite element modeling.

Finite Element Modeling of Adjacent Well Conditions: The casing well is made of iron with a radius of 0.1 m, a depth of 1000 m, and a horizontal section length of 1000 m. There is an adjacent well with a depth of 800 m located 1200 m away in the direction of the horizontal section. The formation has a conductivity of 0.02 S/m, a relative permittivity of 10, a radius of 1000 m, and a depth of 2000 m. An infinite element domain is used. The insulating section is 1 m long, with the casing located 50 m below the insulating section. The potential above the insulating section is 1 V, and the potential below is -1 V. The distribution of electric potential on the ground surface is shown in Figure 13. The ground magnetic flux density is shown in Figure 14, and the radial magnetic flux density with the wellhead of the horizontal well as the origin is shown in Figure 15.

Through the analysis of the above figures, it can be concluded that adjacent wells have a significant impact on the distribution of surface magnetic flux density, while their impact on the ground electric field potential is relatively small. Based on this, magnetic sensor receiving devices can be deployed near the casing of adjacent wells to receive ELF signals while drilling.

2.3. Impact of Field Environmental Noise on Reception

A typical drilling ELF transmission measurement system generally consists of a transmitter, an insulated antenna, a measurement sub, a power supply sub, a drill string, a formation, and a ground receiver (as shown in Figure 16). The downhole measurement system transmits measured wellbore information via the transmitter and insulated antenna, emitting ELF signals that propagate through the formation and drill string to the ground reception system. Since the earth is part of the transmission channel for this system, it is inevitably subject to various types of noise interference related to the formation.

The characteristics of drilling electromagnetic wave noise are mainly related to its generation mode and surrounding environment. During drilling measurement operations, factors such as friction between the drill bit and the formation, vibration of drilling tools, and circulation of drilling fluid can all lead to noise interference, making signal detection difficult (a typical engineering field noise spectrum is shown in Figure 17). Specifically, drilling electromagnetic wave noise mainly originates from external interference noise outside the measurement system and intrinsic noise within the electronic measurement system. External interference noise is diverse, including mud pump noise, drilling noise, pressure fluctuations, and electromagnetic noise. Mud pump noise is often regular, with a frequency similar to the data pulses of the MWD system but potentially larger amplitudes. Drilling noise, generated by the downhole drill bit or power tools, has a broad spectral characteristic. These noise waveforms are time-varying electrical signals with the following characteristics: first, their frequency distribution ranges widely, reflecting the "irregular-

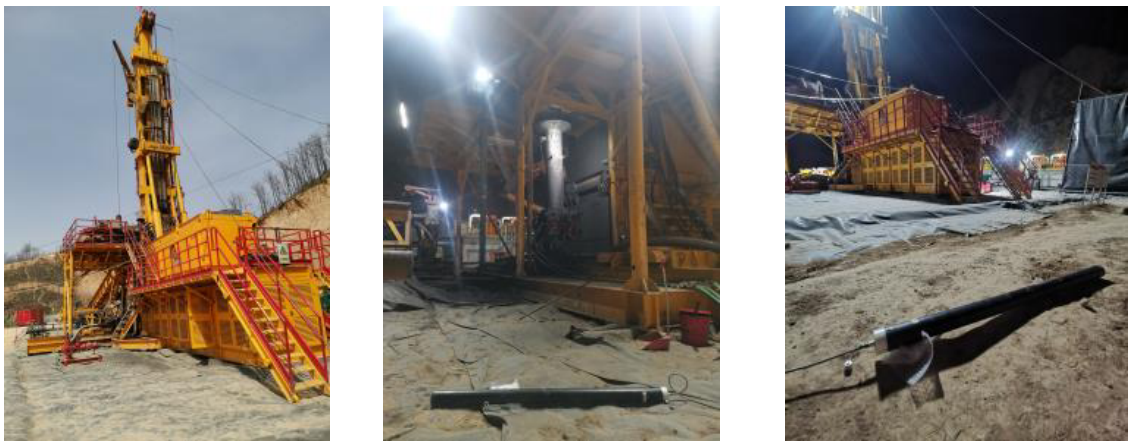

Drilling engineering site | Near-end measurement | Far-end measurement

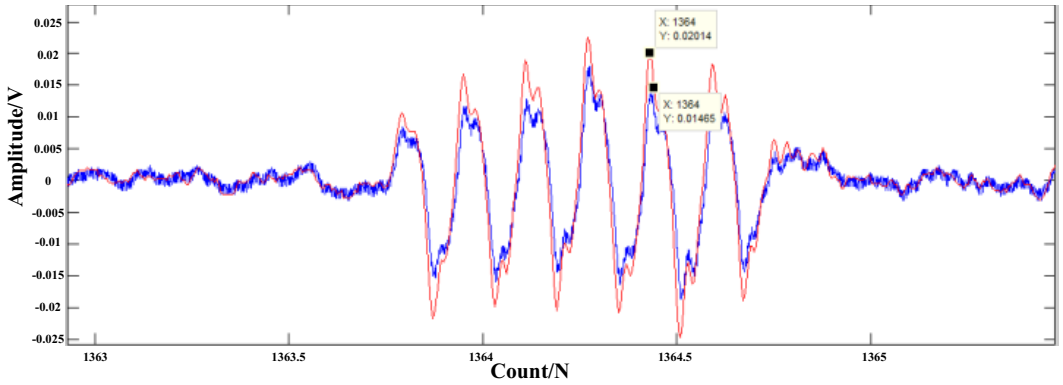

FIGURE 11. Comparison of signal strength at different wiring distances.

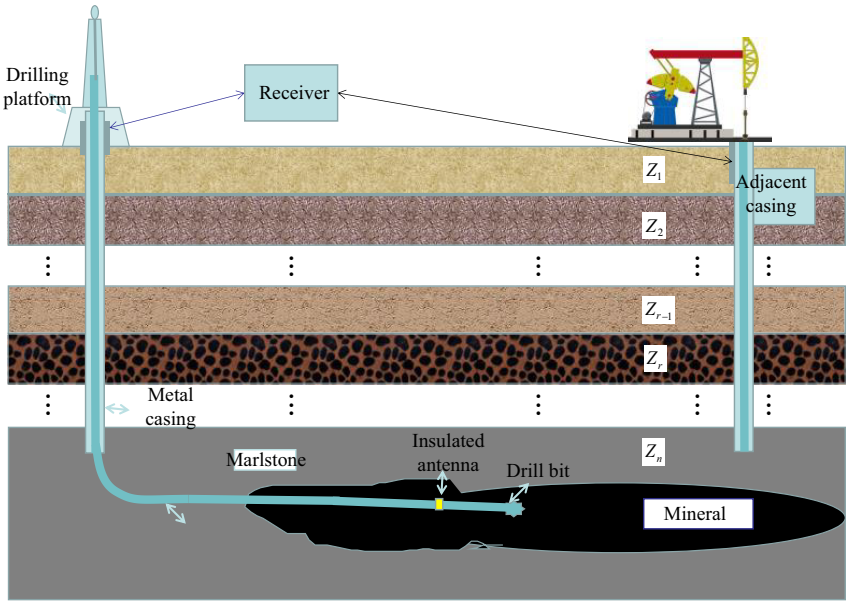

FIGURE 12. Impact of adjacent wells on the EM reception signal at the terminal.

ity" of the noise. Second, the amplitudes of noise signals are random, and even the same type of noise signal can produce different waveforms at different times. This randomness and non-periodicity make noise signals unpredictable. Third, each frequency component in the noise signal has the same energy value, which is an essential characteristic of white noise. To reduce the impact of drilling electromagnetic wave noise on signal detection, it is necessary to analyze the root causes of noise

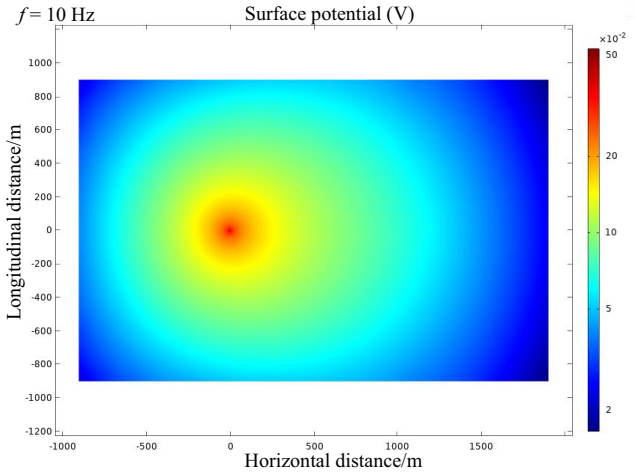

FIGURE 13. Ground potential distribution map in the presence of adjacent wells.

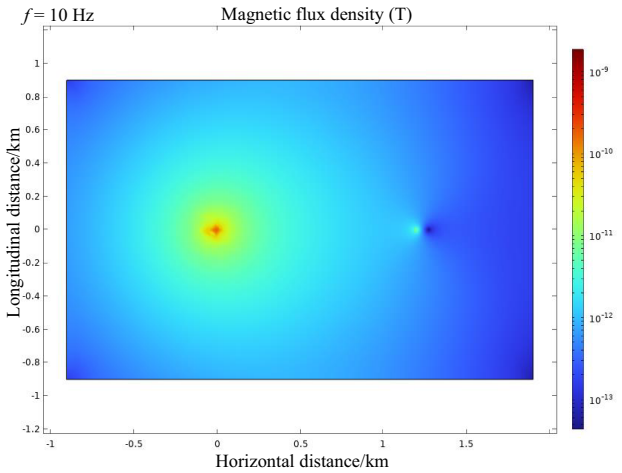

FIGURE 14. Ground magnetic flux density distribution map in the presence of adjacent wells.

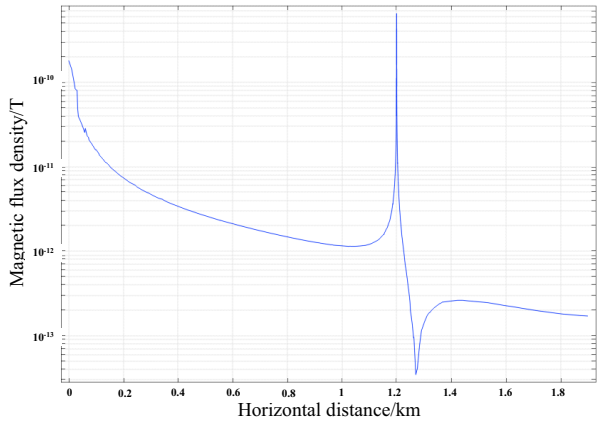

FIGURE 15. Radial magnetic flux density distribution map in the presence of adjacent wells.

and take corresponding measures to eliminate or suppress it, thereby improving signal quality. In general, drilling electromagnetic wave noise is characterized by complexity, randomness, non-periodicity, and uniform energy distribution, posing certain challenges to signal detection [19]. During drilling operations, a series of measures need to be taken to reduce the impact of these noises and ensure the accuracy and reliability of drilling measurement data transmission.

3. MULTI-CHANNEL SIGNAL FUSION INTELLIGENT EXTRACTION ALGORITHM

The noise interference in drilling ELF communication systems can be divided into artificial interference sources and natural interference sources based on their generation mechanisms. Artificial interference is mainly caused by artificial radiation sources such as electromechanical equipment. Natural interference is mainly caused by environmental factors, such as lightning interference and whistler interference, and its impact on receivers varies depending on geographical location. The complexity of noise sources makes it impossible to describe their spectral characteristics in detail. Based on the analysis of these two types of interference sources, interference can be classified into four types in the frequency domain: co-channel interference, near-co-channel interference, out-of-band interference, and random noise interference. Co-channel interference occurs when the interference signal spectrum is within the main frequency band of the desired signal. Near-co-channel interference occurs when the interference signal spectrum is near the cutoff frequency of the main frequency band. Out-of-band interference occurs when the interference signal spectrum is outside the main frequency band. Additionally, there is random noise interference, whose spectrum distribution is similar to that of random white noise, with a broad spectral distribution that affects both within and outside the communication frequency band.

3.1. Single-Channel Multi-Rate Band-Pass Filtering Preprocessing

Typically, narrowband filters are designed to filter out out-of-band noise. In practical engineering, Finite Impulse Response (FIR) digital band-pass filters are commonly used for this purpose due to their linear phase characteristics and relatively easy implementation in both hardware and software. As shown in Figure 18, a FIR digital filter is described using parameter $H(z) = \sum_{k=0}^{N} h(k)z^{-k}$, where $h(k)$ represents the filter coefficients, N the filter order, and z^{-1} the unit delay. The time-domain relationship is expressed as: $y(n) = \sum_{k=0}^{N} h(k)x(n-k)$, where $\mathbf{y}(n)$ and $\mathbf{x}(n)$ are the input and output sequences.

Under the communication conditions of ELF-EM wave transmission, a simulation of the performance of a direct-form FIR band-pass filter is shown in Figure 19. In this simulation, the sampling rate f_s is 1000 Hz, and the filter order is 512.

A multi-rate interpolated FIR band-pass filter $H_{IFIR}(Z)$ is a composite filter that combines a periodic FIR filter $f(z^L)$ with

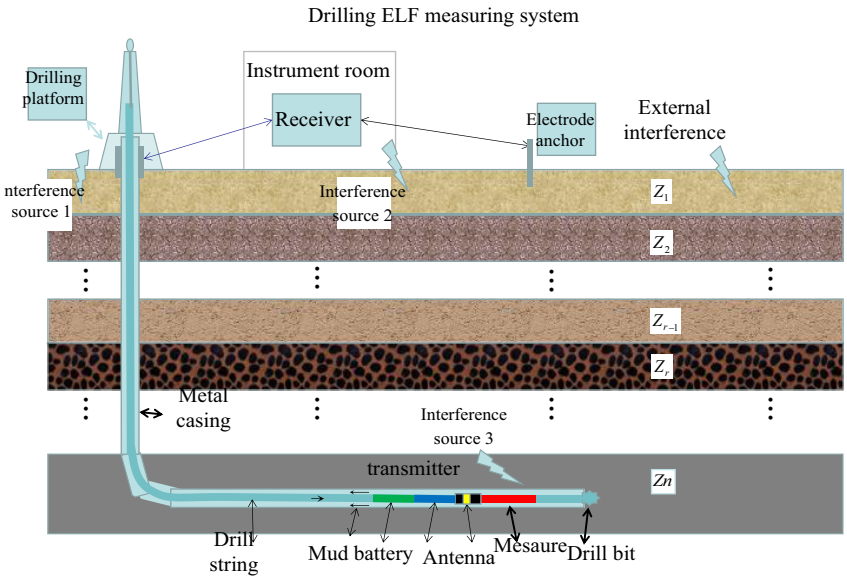

FIGURE 16. Diagram of the drilling ELF measurement system.

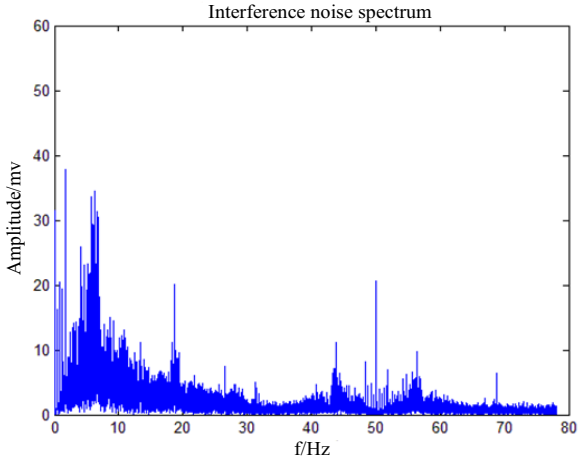

FIGURE 17. Measured spectrum distribution of interference noise in the drilling ELF transmission channel.

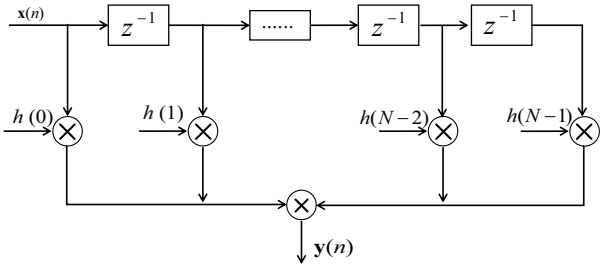

FIGURE 18. Structure diagram of FIR digital filter.

a low-pass filter $I(z)$. Its construction is depicted in Figure 20. The design steps are outlined as follows:

(1) Designing a Shaping Filter $F(z)$

The upper and lower cutoff frequencies of the passband for shaping filter $F(z)$ are $\omega_{p1}^F = L\omega_{p1}$ and $\omega_{p2}^F = L\omega_{p2}$, respectively, while the upper and lower cutoff frequencies of the stopband are $\omega_{s1}^F = L\omega_{s1}$ and $\omega_{s2}^F = L\omega_{s2}$ (where the decimation factor L needs to be calculated and analyzed). The transfer function of the shaping filter F is denoted as: $F(z) = \sum_{n=0}^{N} f(n)z^{-n}$.

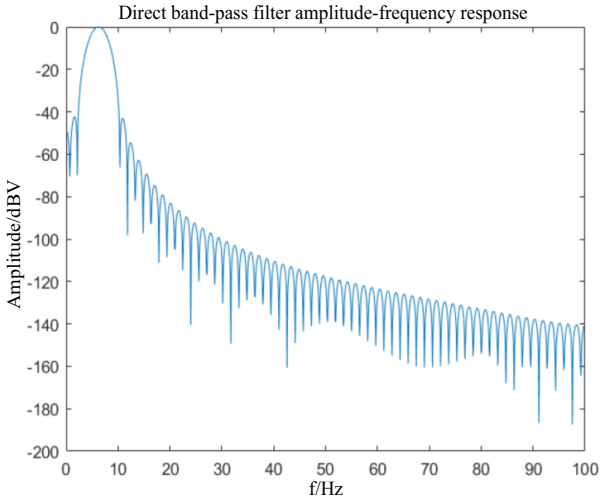

FIGURE 19. Amplitude frequency response diagram of direct-form band-pass filter.

The amplitude-frequency response of Shaping Filter $F(z)$ at this stage is shown in Figure 21.

(2) Designing the Periodic Filter $F(z^L)$

The mathematical expression for the upsampler is:

$$f_u[n] = \begin{cases} f[n/L], & n = 0, \pm L, \pm 2L, \ldots \\ 0, & Others \end{cases} \quad (8)$$

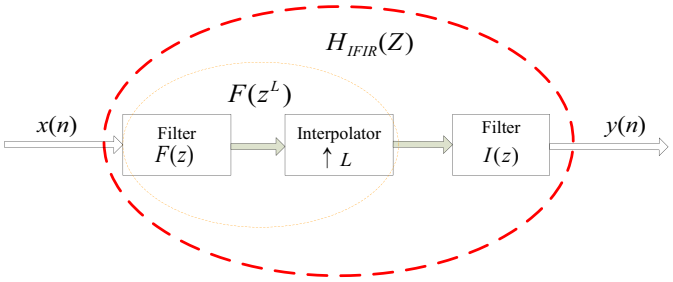

FIGURE 20. Structure diagram of multi-rate interpolation FIR band-pass Filter.

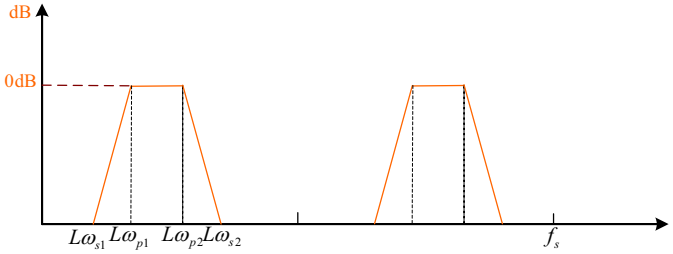

FIGURE 21. Amplitude frequency response diagram of shaping filter $F(z)$.

By cascading the two components, we obtain the periodic filter $F(z^L)$, which can be represented as:

$$F_u(z) = \sum_{n=0}^{NL+1} f_u[n]z^{-n} = \sum_{n=0}^{NL+1} f[n/L]z^{-n}$$

$$= \sum_{m=0}^{N} f[m]z^{-Lm} = F\left(z^L\right) \tag{9}$$

The magnitude frequency response of $F(z^L)$ is illustrated in Figure 22.

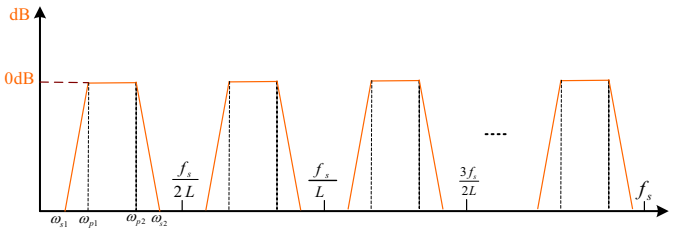

FIGURE 22. Amplitude frequency response diagram of $F(z^L)$.

(3) Designing the Low-Pass Filter $I(z)$

The transition band frequency range of the low-pass filter is $[\omega_{p2}, f_s/L - \omega_{s2}]$, and its magnitude frequency response is shown in Figure 23.

(4) By cascading the periodic filter $F(z^L)$ with the low-pass filter $I(z)$, we obtain the multi-rate FIR filter $H_{IFIR}(Z)$ (as shown in Figure 24).

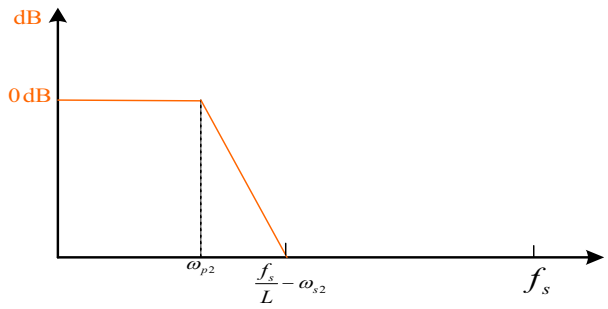

FIGURE 23. Amplitude frequency response diagram of low-pass filter $I(z)$.

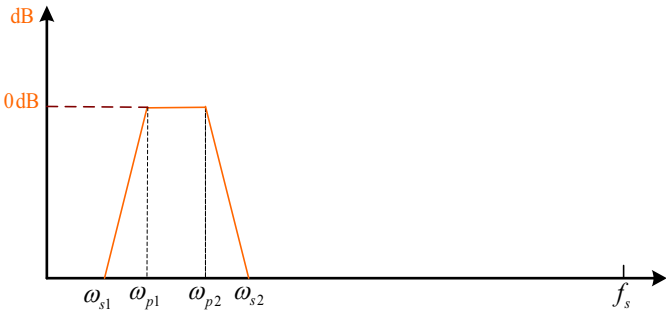

FIGURE 24. Amplitude frequency response diagram of multi-rate filter $H_{IFIR}(Z)$.

The magnitude-frequency characteristic of the multirate filter analyzed theoretically above is shown in Figure 25. This filter utilizes resources equivalent to 256 taps. Under the same resource constraints (in terms of multipliers and adders), the multirate bandpass filter exhibits a steeper transition band than a direct-form FIR bandpass filter, resulting in stronger attenuation of out-of-band noise.

By comparing the magnitude-frequency responses between the direct-form FIR filter in Figure 19 and the multi-rate FIR filter in Figure 24, we can draw the following conclusion: Under the same resource constraints (in terms of multipliers and adders), the multi-rate band-pass filter exhibits superior performance compared to the direct-form FIR band-pass filter, particularly in terms of out-of-band suppression capability. This algorithm offers an improvement of 40 to 50 dB in suppressing out-of-band noise.

3.2. Multi-Channel Signal Fusion and Separation Algorithm

$\mathbf{S} = [s_1(t), s_2(t), \ldots, s_N(t)]^T$ represents the unknown N-dimensional source signal vector, $\mathbf{A}_{M\times N}$ the unknown mixing matrix, $\mathbf{N} = [n_1(t), n_2(t), \ldots, n_M(t)]^T$ the M-dimensional noise vector, and $\mathbf{X} = [x_1(t), x_2(t), \ldots, x_M(t)]^T$ the M-dimensional observed signal (typically measured by receiving antennas or sensors).

$$\mathbf{X} = \mathbf{AS} + \mathbf{N} \tag{10}$$

The goal of Independent Component Analysis (ICA) is to find a separation matrix $\mathbf{W}$ such that each component $\mathbf{Y} =$

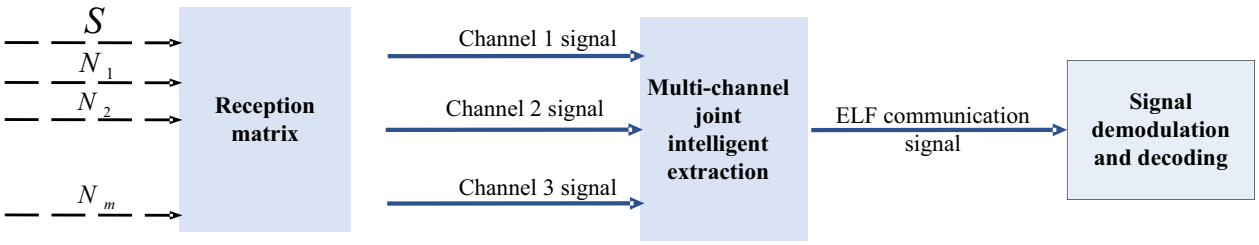

FIGURE 25. Multi-channel signal fusion and extraction.

$[y_1(t), y_2(t), \ldots, y_N(t)]^T$ of $\mathbf{Y}$ is independent.

$$\mathbf{Y} = \mathbf{WX} \tag{11}$$

The FastICA algorithm is based on a fixed-point iterative structure, aiming to maximize the non-Gaussianity of $y = w^T x$. FastICA commonly uses negentropy to measure non-Gaussian random variables. Negentropy can indicate the mutual independence of the separation results. When negentropy reaches its maximum value, the separation process ends. The negentropy of a random variable y is defined as:

$$J(y) = H(y_{gauss}) - H(y) \tag{12}$$

However, calculating negentropy using the above formula is very complex. An approximate estimation can be made using the following formula (13).

$$J(y) \approx \{E[G(y)] - E[G(\upsilon)]\}^2 \tag{13}$$

In Formula (13), υ is a Gaussian random variable with zero mean and unit variance, and G is a non-quadratic function of some form. Specifically, when $G(y) = y^4$, an approximate solution based on kurtosis is obtained.

The derivation of the FastICA algorithm is as follows [20]:

First, the fixed-point iterative method is introduced:

$$\mathbf{w} = E\left\{\mathbf{v}g(\mathbf{w}^T\mathbf{v})\right\} \tag{14}$$

where $\mathbf{v}$ is the data obtained by whitening the observed variable $\mathbf{x}$, and g is the derivative of the non-quadratic function G, with the following relationship:

$$g_1(y) = \tanh(a_1 y) \tag{15}$$

$$g_2(y) = y \cdot \exp(-y^2/2) \tag{16}$$

$$g_3(y) = y^3 \tag{17}$$

a_1 is a constant, typically within the range of $1 \le a_1 \le 2$, and can be set to $a_1 = 1$. Adding $a\mathbf{w}$ to both sides of Equation (14):

$$(1+a)\mathbf{w} = E\left\{\mathbf{v}g(\mathbf{w}^T\mathbf{v})\right\} + a\mathbf{w} \tag{18}$$

The coefficient a can be obtained through the Newton approximation method. According to the Kuhn-Tucker conditions, under the constraint condition of $E\left\{(\mathbf{w}^T\mathbf{v})^2\right\} = \|\mathbf{w}\|^2 = 1$, the optimal value of $E\left\{G(\mathbf{w}^T\mathbf{v})\right\}$ is obtained through the following formula:

$$E\left\{yg(\mathbf{w}^T\mathbf{v})\right\} + \beta\mathbf{w} = 0 \tag{19}$$

In the above formula, β is a constant, and its Jacobian matrix is:

$$J\left\{F(\mathbf{w})\right\} = E\left\{\mathbf{v}\mathbf{v}^T g(\mathbf{w}^T\mathbf{v})\right\} + \beta\mathbf{I} \tag{20}$$

The first term on the left side of the above formula can be approximated as:

$$E\left\{\mathbf{v}\mathbf{v}^T g(\mathbf{w}^T\mathbf{v})\right\} \approx E(\mathbf{v}\mathbf{v}^T)E\left\{g(\mathbf{w}^T\mathbf{v})\right\} = E\left\{g(\mathbf{w}^T\mathbf{v})\right\}\mathbf{I} \tag{21}$$

Based on this, according to Lagrange's theorem and its constraint conditions, we can obtain:

$$w_i(k+1) = w_i(k) - [E\left\{zg(w_i^T(k)v)\right\} + \beta w_i(k)]/[E\left\{g'(w_i^T(k)v)\right\} + \beta] \tag{22}$$

The above formula can be further simplified to:

$$w_i(k+1) = E\left\{vg(w_i^T(k)v)\right\} - E\left\{g'(w_i^T(k)v)\right\} w_i(k) \tag{23}$$

The steps of FastICA are summarized as follows:

(1) Center the data to make its mean zero;

(2) Whiten the data to obtain $\mathbf{v}$;

(3) Select an initialization vector $\mathbf{w}$ with unit norm;

(4) Update

$$w_i(k+1) = E\left\{vg(w_i^T(k)v)\right\} - E\left\{g'(w_i^T(k)v)\right\} w_i(k);$$

(5) Standardize

$$w_i(k+1) = w_i(k+1)/\left\|w_i(k+1)\right\|;$$

(6) If not converged, return to step (4) and continue iterating.

3.3. Intelligent Signal Extraction Based on Maximum Signal-to-Noise Ratio Estimation

SNR estimation plays an irreplaceable role in DSP and communication systems. For instance, in adaptive equalization algorithms, the decision-directed approach requires SNR estimation of the desired signal to update the adaptive filter coefficients. Additionally, in multi-channel diversity combining algorithms, SNR estimation for each channel is necessary to achieve a better combining effect.

Assuming the actually acquired signal is represented as: $y(t) = s(t) + n(t)$, with power spectral density $Y(f)$, then the total power within the bandwidth is:

$$P = \int_{f_L}^{f_H} Y(f)df \tag{24}$$

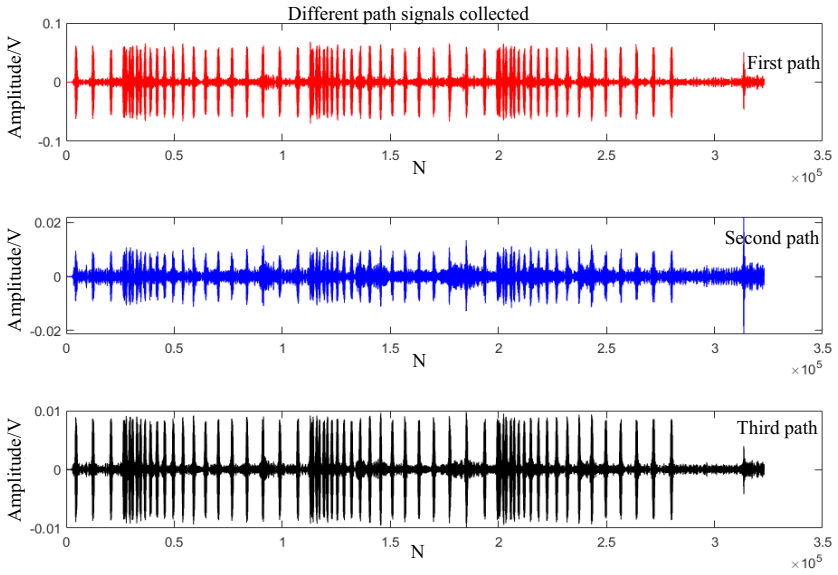

FIGURE 26. Three-channel data with high signal-to-noise ratio collected on site (before processing).

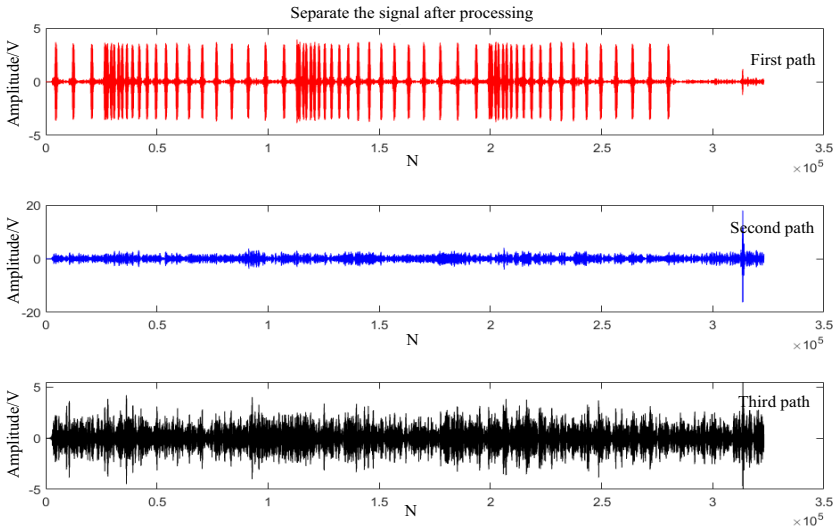

FIGURE 27. Three-channel data with high signal-to-noise ratio collected on site (after processing).

where f_L and f_H denote the start and end frequencies of the effective bandwidth, respectively.

$$P_{all} = \int_{f_1}^{f_2} Y(f)df \tag{25}$$

f_1 and f_2 represent the start and end frequencies of sampling.

Furthermore, the noise density estimate can be obtained as:

$$n_0 = \frac{P_{all} - P}{B - B_w} \tag{26}$$

where $B = F_1 - F_2$ represents the sampling bandwidth, and B_w denotes the useful signal bandwidth.

The SNR estimate is given by:

$$\overline{SNR} = 10 * \lg\left(\frac{P - N}{n_0 * B}\right) \tag{27}$$

where $N = n_0 * B_w$ is the noise power. This SNR estimation algorithm is typically used for estimating SNR in signals containing random noise.

In this paper, the following scheme is adopted for intelligent extraction of multi-channel signals (as shown in Figure 25), with the final extracted signal data having an SNR superior to that of any single-channel data. Taking the electric field channel as an example, assume that three electric field signals arrive at the receiver terminal through different channel polarizations. After synchronization by the internal circuitry, the previously mentioned FastICA is used for signal separation. Then, SNR estimation is performed on each of the separated signals. Based on the maximum SNR criterion, ELF communication signals are extracted. Finally, the extracted signals are demodulated and decoded.

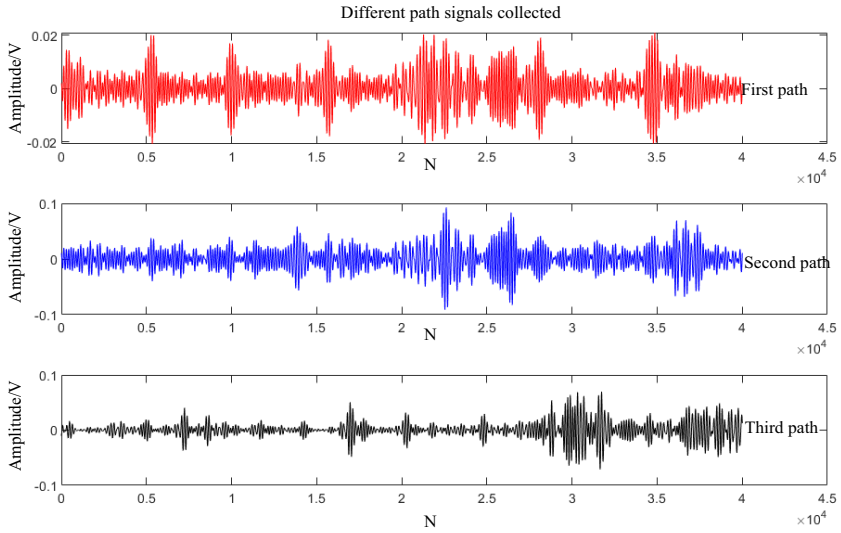

FIGURE 28. Three-channel data with low signal-to-noise ratio collected on site (before processing).

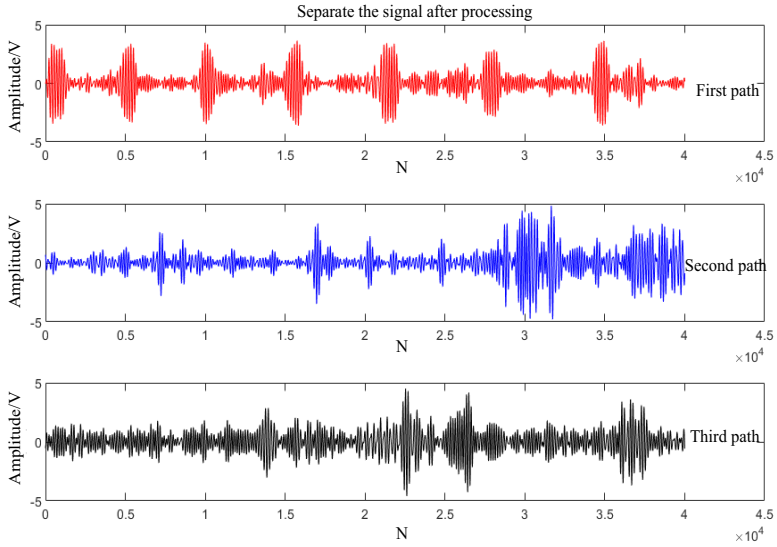

FIGURE 29. Three-channel data with low signal-to-noise ratio collected on site (after processing).

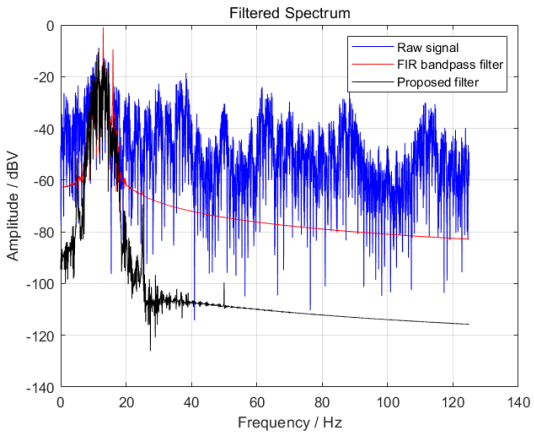

FIGURE 30. Spectral comparison between the proposed and conventional filtering methods.

4. VERIFICATION WITH REAL FIELD DATA

The engineering effectiveness of the proposed method is illustrated through two sets of field data. Figures 26 and 27 present a comparison of three-channel data with relatively good signal-to-noise ratios (SNRs) before and after separation, while Figures 28 and 29 show a comparison for three-channel data with poorer SNRs. It is important to note that the first channel of data after separation corresponds to the ELF communication data that needs to be isolated. The results demonstrate that the multichannel signal data fusion scheme can significantly improve the SNR of the signals. Calculations show that in cases of poor signal quality, the SNR (approximately in-band SNR) can be increased by more than 3 to 5 dB, thereby laying a solid foundation for demodulation and decoding (Figure 30 compares the signal spectra of proposed and conventional methods, and Figure 31 contrasts the transmitted and received symbol sequences by different approaches). According to signal transmission the-

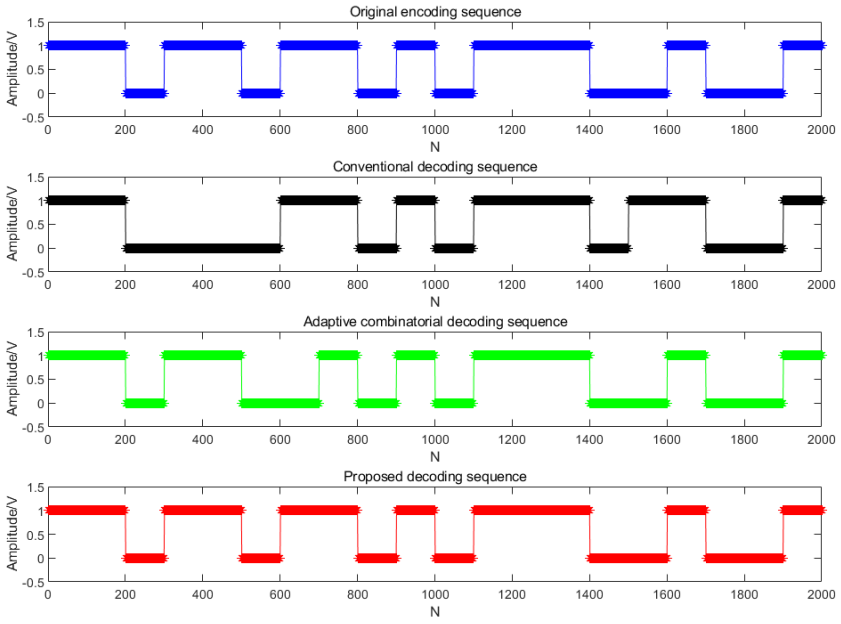

FIGURE 31. Comparison of the transmitted and received symbol sequences between the proposed method and the traditional method.

ory, in areas suitable for electromagnetic wave transmission (with loads above 10 ohms), estimating a signal attenuation of 2 to 3 dB per hundred meters [20], this scheme theoretically allows for an increase in transmission distance by 100 to 150 meters.

5. CONCLUSION

ELF technology plays a crucial role in the exploration and development of mineral resources such as oil and natural gas. ELF drilling communication technology, characterized by its fast signal transmission speed, high measurement accuracy, and the ability to transmit electromagnetic waves without requiring specific media and being unaffected by drilling fluids, has emerged as a significant development direction in MWD technology. Among its components, intelligent signal extraction is a pivotal aspect directly related to the accuracy and reliability of data. In actual drilling wireless communication, the ELF signal faces an exceptionally complex electromagnetic distribution on the ground surface. Its transmission distance and attenuation characteristics are influenced by physical parameters such as formation conductivity and permittivity, and its transmission path may be affected by factors such as formation structure, rock type, and water content, leading to the attenuation of signal strength and changes in phase. This paper utilizes the finite element analysis method to analyze the surface electromagnetic field distribution of ELF communication signals in large-displacement horizontal wells under different drilling conditions, determining the optimal signal reception method at the drilling site.

Regarding terminal signal extraction, ELF signals received on the ground inevitably suffer from the impact of formation and engineering factors due to the time-varying and strong noise characteristics of ELF formation transmission channels. In particular, in-band noise more easily affects the final decoding effect of the instrument, ultimately resulting in a high bit error rate and inaccurate decoding of detected formation information. This paper transitions from traditional single-channel reception to multi-channel reception technology and designs an intelligent signal extraction algorithm. Compared to traditional single-channel reception, the in-band SNR can be improved by 3 to 5 dB, effectively increasing the communication transmission distance.

Intelligent signal extraction for ELF electromagnetic MWD is an engineering problem involving multiple technical fields. Continuous optimization of technical methods and addressing technical challenges are required to provide more reliable and efficient support for the exploration and development of mineral resources. Future improvements can be attempted in the following aspects: (1) Optimizing the transmission system and improving encoding methods, such as adaptively optimizing transmitter parameters based on formation resistivity and incorporating channel error correction codes to enhance terminal SNR; (2) Introducing advanced artificial intelligence algorithms into engineering applications.

ACKNOWLEDGEMENT

This work was supported by the Stable-Support Scientific Project of China Research Institute of Radiowave Propagation(Grant No. A132301213) and the Foundation of National Key Laboratory of Electromagnetic Environment (Grant No. JCKY2023210C614240301).

REFERENCES

[1] Liang, P., Q. Di, Q. Zhen, R. Wang, O. Fayemi, C. Fu, D. Lei, Z. An, J. Fan, Z. Ma, and L. Yang, "Electromagnetic telemetry simulation in vertical drillings," *Geophysics*, Vol. 85, No. 6, E207–E219, 2020.

[2] Liu, R., W. Zhang, W. Chen, P. Liang, W. Liu, and X. Li, "Analysis and experimental research on the factors affecting downhole inductive electromagnetic wave wireless short-hop transmission," *IEEE Transactions on Geoscience and Remote Sensing*, Vol. 62, 1–11, 2024.

[3] Wang, W.-J., W.-Q. Li, Y.-H. Wu, C.-M. Liu, Y.-Q. Ma, L. Lin, M. Peng, G.-H. Zhang, and L.-C. Zhong, "Study on surface electromagnetic wave transmission properties based on logging while drilling," in *International Field Exploration and Development Conference*, 6889–6900, Springer, Singapore, 2022.

[4] Fan, Y., Z. Nie, and T. Li, "EM channel theory model and characteristics analysis for MWD," *Chinese Journal of Radio Science*, Vol. 28, No. 5, 909–914, 2013.

[5] Liang, P. F., Q. H. Zhen, Z. Yun, C. M. Fu, R. Wang, and Q. Y. Di, "Accurate and fast simulation of electromagnetic waves for well-to-ground transmission in transverse isotropic media," *Chinese Journal of Geophysics*, Vol. 66, No. 1, 122–130, 2023.

[6] Li, F. K., J. Chen, and Y. L. Ji, "Analysis on the application of electromagnetic wave while drilling in the identification of minerals," *Chinese Journal of Radio Science*, Vol. 37, No. 3, 449–456, 2022.

[7] Liu, K., "Model and control method of a downhole electromagnetic transmitter for EM-MWD system," *Journal of Petroleum Science and Engineering*, Vol. 192, 107210, 2020.

[8] Li, W., Z. Nie, X. Sun, and Y. Chen, "Numerical modeling for excitation and coupling transmission of near field around the metal drilling pipe in lossy formation," *IEEE Transactions on Geoscience and Remote Sensing*, Vol. 52, No. 7, 3862–3871, 2013.

[9] Zhang, C., H. Dong, J. Ge, and H. Liu, "Theoretical channel model and characteristics analysis of EM-MWD in the underground coal mine," *IEEE Access*, Vol. 9, 142 644–142 652, 2021.

[10] Wang, P. and Z. Hu, "Numerical simulation analysis of electromagnetic wave transmission characteristics in open hole well," *International Core Journal of Engineering*, Vol. 10, No. 2, 162–171, 2024.

[11] Long, L., Q. Chen, and F. Liu, "Research on eliminating interference signal algorithm of EM-MWD," *Chinese Journal of Scientific Instrument*, Vol. 35, No. 9, 2144–2152, 2014.

[12] Wang, H., H. Dong, and G. Jiang, "Design of EM-MWD signal detection system based on correlation and adaptive filter," *Chinese Journal of Scientific Instrument*, Vol. 33, No. 05, 1013–1018, 2012.

[13] Fayemi, O., Q. Di, Q. Zhen, and P. Liang, "Demodulation of EM telemetry data using fuzzy wavelet neural network with logistic response," *Applied Sciences*, Vol. 11, No. 22, 10877, 2021.

[14] Lu, C., T. Zhang, and H. Zhao, "Improving the application depth of electromagnetic measurement while drilling (EM-MWD) systems by receiving signals from adjacent wells," *Journal of Applied Geophysics*, Vol. 195, 104468, 2021.

[15] Shao, C., L. Xu, X. Chen, Z. Chu, and B. Yang, "Factors affecting received signal intensity of electromagnetic measurement-while-drilling during underground in-seam horizontal drilling," *Journal of Natural Gas Science and Engineering*, Vol. 56, 212–221, 2018.

[16] Shao, C., X. Fu, and J. Zhang, "ANSYS simulation analysis on the influence of drill string on EM-MWD signal transmission of surface borehole," *Coal Geology & Exploration*, Vol. 44, No. 3, 128–131, 2016.

[17] Jiang, T., K. Ma, H. Li, Q. Chen, X. Han, D. Pang, and Q. Wang, "Research on wireless transmission performance of near-drill magnetic field," in *2020 IEEE 1st China International Youth Conference on Electrical Engineering (CIYCEE)*, 1–5, Wuhan, China, 2020.

[18] Zhang, H., X. Bi, W. Liu, Y. Xu, M. Song, and S. Shao, "Investigation of the factors that influence EM-MWD signal transmission in drill strings," *Petroleum Drilling Techniques*, Vol. 49, No. 6, 125–130, 2021.

[19] Li, F., J. Wu, J. Chen, H. Peng, and Y. Fan, "ELF-EM signal processing while drilling based on human-computer interaction combined algorithm," *China Communications*, Vol. 20, No. 6, 178–198, 2023.

[20] Liu, M., S. Li, S. Liu, G. Guo, M. Cai, and Z. Dai, "Leak location for urban elbowed water pipe based on complex-optimized FastICA blind deconvolution," *IEEE Sensors Journal*, Vol. 23, No. 4, 4033–4042, 2023.